



Seismic data analysis for subglacial lake D2 beneath David Glacier, Antarctica

Hyeontae Ju^{1,2}, Seung-Goo Kang³, Yeonjin Choi³, Sukjoon Pyun², Min Je Lee³, Hoje Kwak⁴, Kwansoo Kim¹, Yeadong Kim⁵, Jong Ik Lee³

¹Center of Technology Development, Korea Polar Research Institute, Incheon 21990, Korea

²Department of Energy Resource Engineering, Inha University, Incheon 22212, Korea

³Division of Glacier & Earth Sciences, Korea Polar Research Institute, Incheon 21990, Korea

⁴Unit of Antarctic Inland Research, Korea Polar Research Institute, Incheon 21990, Korea

⁵Korea National Committee on Polar Research, Incheon 21990, Korea

Correspondence to: Seung-Goo Kang (ksg9322@kopri.re.kr)

Abstract. Subglacial lakes beneath Antarctic glaciers are pivotal in advancing our understanding of cryosphere dynamics, basal hydrology, and microbial ecosystems. We investigate the internal structure and physical properties of Subglacial Lake D2 (SLD2), located beneath David Glacier in East Antarctica, using seismic data acquired during the 2021/22 austral summer. The dataset underwent a comprehensive processing workflow, including noise attenuation, velocity analysis, and pre-stack time migration. Migrated seismic sections revealed distinct reverse- and normal-polarity reflections at the glacier–lake and lake–bed interfaces, respectively. We compared the synthetic seismogram generated through wave propagation modelling based on our structural interpretation of the migrated sections with the field data to validate the subglacial lake structure inferred from the seismic data. This confirmed a water column thickness ranging from around 53 to 82 m and delineated the broader structure of the subglacial lake. Also, discontinuous reflections detected on seismic sections transverse to the ice flow were interpreted as scour surfaces formed by ice movement. Comparison with airborne ice-penetrating radar (IPR) data acquired in 2018 further supported the consistency of the ice thickness estimates. Notably, a steeply dipping bedrock boundary identified along profile 21YY provided a more precise definition of the lateral extent of SLD2 than was possible using IPR data alone. Collectively, these findings enhance our understanding of subglacial lake environments and inform the selection of future drilling sites for in situ sampling.

1 Introduction

Subglacial lakes beneath the Antarctic Ice Sheet are typically overlain by glaciers several kilometers thick and have remained isolated from direct atmospheric and solar influences for millions of years, creating extreme environments characterized by low temperatures (Thoma et al., 2010) and high pressures (Tulaczyk et al., 2014). With increasing scientific interest, subglacial



lakes have become a focal point for studies related to the Antarctic paleoclimate, as inferred from lake sediments, as well as investigations into microbial life in polar ecosystems (Bell et al., 2007, 2011; Bentley et al., 2009; Christner et al., 2014; Engelhardt et al., 1990; Priscu and Christner, 2003; Rose, 1979; Wingham et al., 2006). Additionally, these lakes influence glacier dynamics by reducing basal friction, facilitating ice flow, and potentially accelerating calving events (Bell et al., 2007; Stearns et al., 2008; Winsborrow et al., 2010). Characterizing subglacial lakes is essential for understanding cryospheric processes, reconstructing past climate conditions, and assessing the potential for life in isolated, extreme environments.

The sampling of subglacial lake water, sediments, and microbial communities is critical to address these scientific objectives. However, successful sampling requires careful selection and characterization of the drilling site. Airborne ice-penetrating radar (IPR) surveys are commonly employed at regional scales to detect potential subglacial lake suitable locations for drilling (Christianson et al., 2012; Lindzey et al., 2020; Yan et al., 2022). However, due to signal attenuation in water, IPR surveys are limited in resolving the internal structure of subglacial lakes. To overcome this limitation, seismic surveys have been conducted at potential subglacial lake candidates identified from IPR surveys. During such surveys, P-waves propagate through the water column and are partially reflected at the lake–bed interface because of contrasts in acoustic impedance. Analyzing these reflected waves enables detailed delineation of the water column and underlying substrate, thereby informing optimal drilling locations (Brisbourne et al., 2023; Filina et al., 2008; Horgan et al., 2012; Woodward et al., 2010).

As such, numerous studies have utilized seismic surveys to investigate the characteristics of subglacial lakes, including Subglacial Lake Ellsworth, Subglacial Lake Whillans, and Subglacial Lake CECs. Subglacial Lake Ellsworth, located beneath 2,930–3,280 m of glacial ice in West Antarctica, was the subject of a seismic survey during the austral summer of 2007–08. This survey revealed spatially variable ice thickness and a lake water column ranging from 52 to 156 m, which guided the identification of an optimal drilling location (Smith et al., 2018; Woodward et al., 2010). Subglacial Lake Whillans lies beneath approximately 800 m of ice. Seismic observations conducted during the 2010/11 field season revealed water columns extending over a 5 km segment of the survey profile, with a maximum thickness of less than 8 m. The glacier bed was predominantly composed of soft sediments, and localized zones with shallow water columns (< 2 m) were also identified (Horgan et al., 2012). Subsequent drilling in the summer of 2012/13 confirmed the presence of microbial life in both the water and sediment samples (Christner et al., 2014). Subglacial Lake CECs (SLCECs), located beneath 2653 m of ice at the Rutford–Institute–Minnesota Divide in West Antarctica, were investigated through seismic surveys conducted in the 2016/17 and 2021/22 seasons. These surveys revealed a maximum water column thickness of 301.3 ± 1.5 m and clastic sediments up to 15 m thick covering the lakebed. While the lake center was relatively flat, significant topographic variability was observed near the lake margins (Brisbourne et al., 2023).

We have initiated subglacial lake research beneath David Glacier, the closest major glacier to Jang Bogo Station in East Antarctica. Satellite altimetry has identified six subglacial lakes in this region (Smith et al., 2009; Wright and Siegert, 2012). During the 2016/17 austral summer, an airborne IPR survey was conducted over the region encompassing Subglacial Lake D1 (SLD1) and Subglacial Lake D2 (SLD2) (Lindzey et al., 2020). A subsequent high-resolution IPR survey was carried out during the 2018/19 field season, focusing solely on SLD2 (Frémand et al., 2023; Ju et al., 2024b). The combined results of the



two surveys revealed moderately enhanced radar bed echoes relative to the surrounding area, specularities values (>0.4), a depressed basal elevation (≤ -350 m), and a low hydraulic gradient ($\leq 0.84^\circ$), collectively indicating a high potential for the presence of subglacial water beneath SLD2. Seismic surveys were employed to investigate the structure of the lake further. In the 2019/20 season, an initial seismic campaign identified the glacier thickness and suggested the presence of the lake; however, the data quality was compromised by surface crevasse noise and a lack of adequate fold coverage, limiting detailed interpretation. A refined seismic survey with 8-fold coverage was conducted during the 2021/22 season to address these issues. In this study, we present a detailed analysis of the physical and structural properties of SLD2 using seismic data acquired during the 2021/22 campaign. We first describe the seismic data processing workflow, including noise attenuation, amplitude correction, and pre-stack time migration. The final results reveal seismic reflections corresponding to the glacier-lake and lake-bed interfaces. Subsequently, the seismic interpretation is validated through comparison with synthetic seismograms, and a quantitative analysis is performed to determine key structural characteristics of SLD2, including ice thickness, water column thickness, and basal structure of the lake.

2 Subglacial Lake D2 Beneath David Glacier in Antarctica

2.1 David Glacier

David Glacier, located in Victoria Land, East Antarctica, originates from the Dome C and Talos Dome regions and flows seaward through the Drygalski Ice Tongue (Fig. 1). The mass balance of the glacier from 1979 to 2008 has been estimated at 7.5 ± 0.4 Gt yr⁻¹ (Rignot et al., 2019), while the mean ice discharge over the more extended period from 1979 to 2017 was reported to be approximately 9.7 Gt yr⁻¹ (Frezzotti et al., 2000; Rignot et al., 2019). These estimates suggest that ice discharge exceeds net accumulation, indicating a negative mass balance and implying that David Glacier has contributed to global sea-level rise.

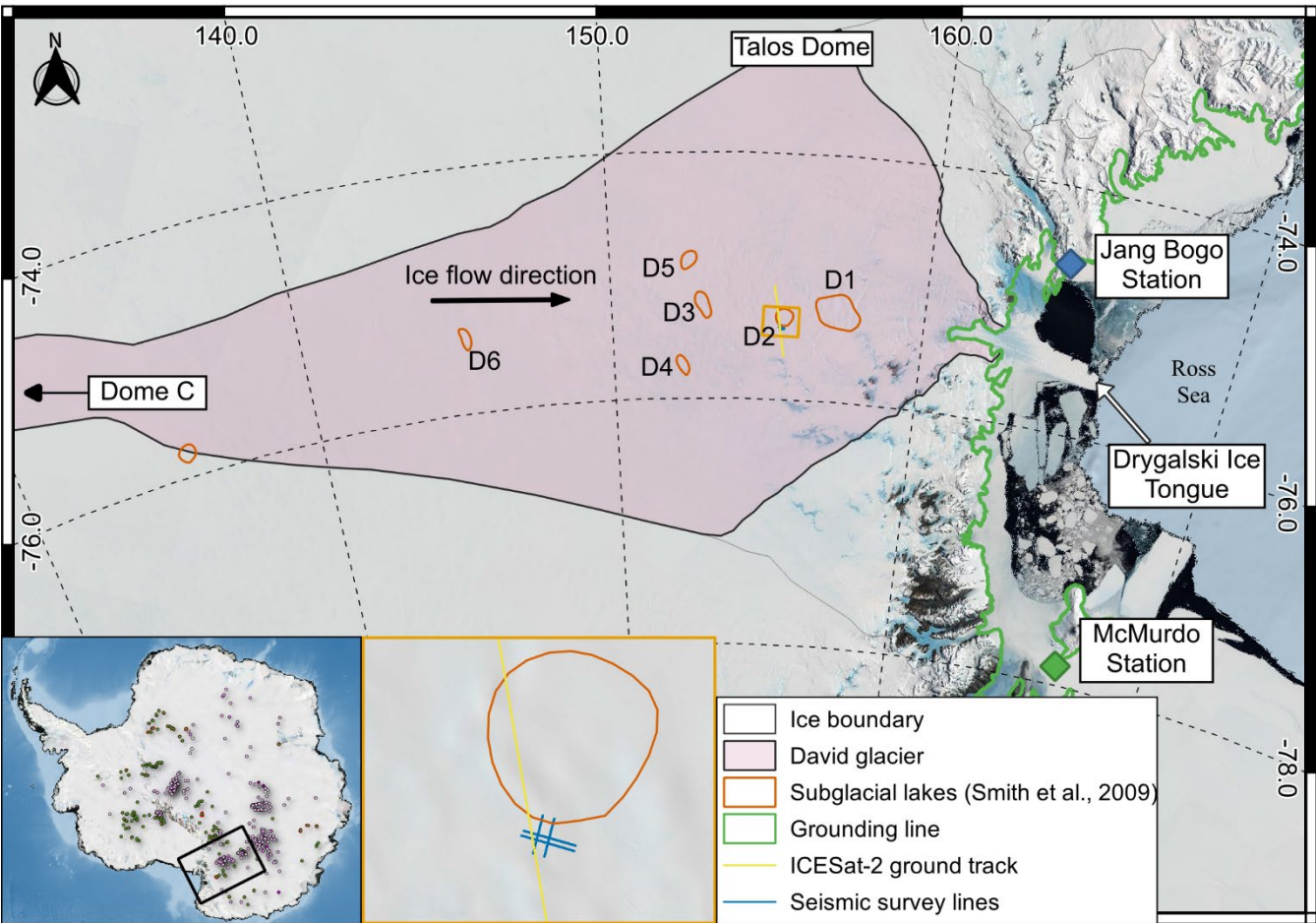


Figure 1: Locations of subglacial lakes D1–D6 in the David Glacier region, Victoria Land, Antarctica (EPSG: 4326–WGS84).

2.2 Subglacial Lake D2

Subglacial lakes in Antarctica are generally categorized as either stable or active. Approximately 80% of subglacial lakes in Antarctica are classified as stable subglacial lakes. These closed systems do not exhibit significant surface elevation changes, and where subglacial water remains largely isolated, with minimal exchange due to slow and stable recharge and discharge cycles. The remaining 20% are classified as active subglacial lakes, which exhibit surface elevation changes due to episodic water drainage and refilling events (Livingstone et al., 2022).

Among the six subglacial lakes (D1–D6) identified beneath David Glacier via satellite altimetry (Smith et al., 2009; Wright and Siegert, 2012), SLD2 was observed to have experienced a drainage event between 2003 and 2008 based on ICESat altimetry data (Smith et al., 2009). Since the drainage event, a continuous increase in surface elevation over SLD2 has been observed, indicating water refilling, as detected from CryoSat-2 altimetry data (2013–2017) (Siegfried and Fricker, 2018) and



more recently from ICESat-2 observations (2019–2024) (Fig. 2). Figure 2 shows elevation changes relative to April 2019, indicating surface uplift through January 2022. After this period, the surface elevation remained stable in the region originally delineated as SLD2 (Smith et al., 2009), whereas the seismic survey region experienced a decreased elevation. These patterns of elevation change strongly suggest that SLD2 is an active subglacial lake, with cyclic drainage and refilling likely contributing to the presence of subglacial sediments.

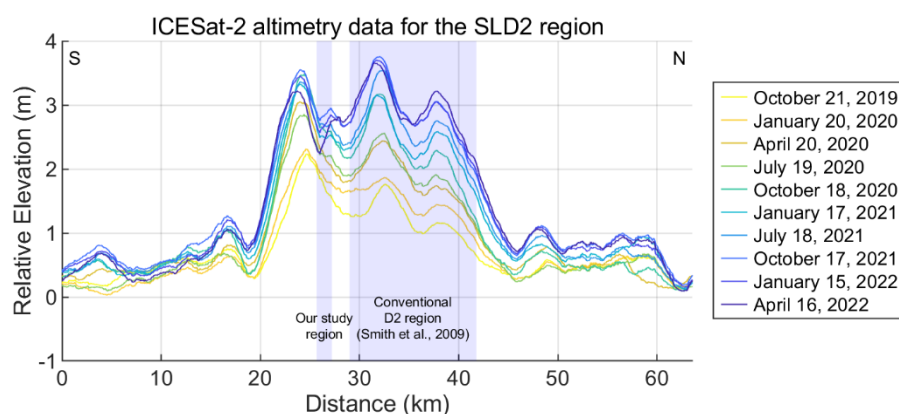


Figure 2: Glacier surface elevation changes derived from ICESat-2 altimetry between 22 April 2019 and 12 July 2024. The X-axis corresponds to the 22 April 2019 dataset, and all subsequent elevation changes are referenced to this date. The light blue shaded region indicates the spatial overlap between the conventional SLD2 region identified by Smith et al. (2009) and our study region.

Airborne IPR surveys were conducted during the 2016/17 and 2018/19 austral summer seasons to better constrain the lake's extent and basal conditions. These surveys indicate that glacier surface elevations in the SLD2 region range from 1820 to 1940 m, with ice thicknesses varying between 1685 and 2293 m. Furthermore, the observations of moderately enhanced radar bed echoes relative to the surrounding area, elevated specularities (>0.4), depressed basal elevations (≤ -350 m), and low hydraulic gradients ($\leq 0.84^\circ$) collectively suggest a high potential for the presence of subglacial water beneath SLD2. (Frémand et al., 2023; Ju et al., 2024b; Lindzey et al., 2020).

3 Method

3.1 Seismic survey

As previously noted, the internal structure and water column of subglacial lakes cannot be fully resolved using IPR alone because of signal attenuation in water. Accordingly, a seismic survey was conducted within the candidate SLD2 region identified from IPR data to investigate the structure of the subglacial lake more precisely. A preliminary seismic survey conducted during the 2019/20 austral summer confirmed both the glacier thickness and the presence of subglacial water, providing critical guidance for the subsequent detailed survey conducted during the 2021/22 season. For the refined survey,



seismic acquisition lines were planned using bed topography derived from IPR and surface elevation data from satellite altimetry. A total of four seismic lines were deployed and designated 21X, 21Y, 21XX, and 21YY (Fig. 3). Lines 21X and 21XX, oriented approximately 52° relative to the ice flow direction, are situated at an average surface elevation of 1894 ± 13 m. Lines 21Y and 21YY, oriented approximately -30° in the ice flow direction, lie at an average elevation of 1887 ± 16 m. All lines traverse regions of minimal topographic relief, with average surface slopes of approximately 0.5° , indicating a relatively flat and stable glacier surface. The lengths of the 21X/21XX and 21Y/21YY lines are approximately 5 km and 3.5 km, respectively. Seismic acquisition for lines 21X and 21Y was conducted using 8-fold coverage to increase the resolution, whereas lines 21XX and 21YY were acquired with 4-fold coverage due to time constraints during the survey. The additional acquisition parameters are summarized in Table 1.

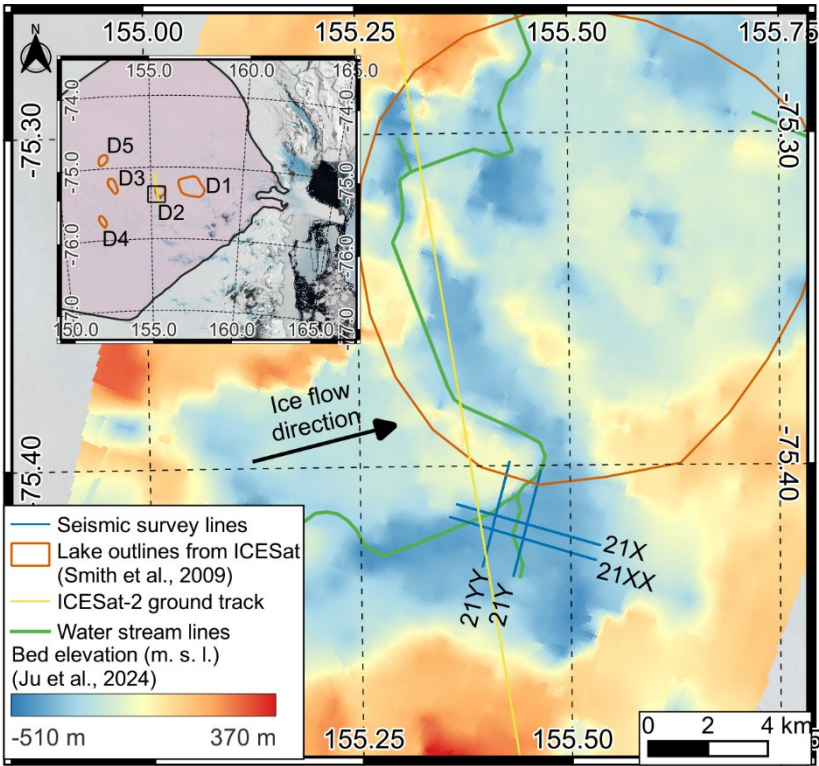


Figure 3: Seismic survey layout (blue lines) overlaid on bed elevation data from IPR results (Ju et al., 2024b).

Table 1: Parameters of the active-source seismic survey.



Survey Parameters		Survey lines			
		21X line	21Y line	21XX line	21YY line
Line length (km)		5	3.5	5	3.5
Fold		8	8	4	4
Shot interval (m)		90	90	180	180
Number of shots		56	40	28	20
Receiver channels				96	
Receiver interval (m)				15	
Recording time (s)				4	
Record peak frequency (kHz)				1	
Record sampling rate (ms)				0.25	
Survey time (days)				34	
Survey crew size			Hot water drilling (3), Seismic (6)		

Before the seismic survey, a ground-penetrating radar (GPR) survey was used to identify the firm transition zone at depths of approximately 20–22 m. To enhance seismic signal transmission, 1.6 kg of pentaerythritol tetranitrate (PETN) explosives were emplaced at depths of 25–30 m using hot water drilling techniques. A total of 144 shots were deployed across the four survey lines. Given the snow-covered glacier surface, Georods were used instead of conventional spike-type geophones to increase signal detection efficiency (Voigt et al., 2013). Each Georod houses four geophone elements in a 0.6 m-long cylindrical array, producing a single output by summing the inputs from all the elements. Compared with traditional geophones, this configuration improves coupling and detection performance in snow-dominated environments (Ju et al., 2024a). Figure 4 presents shot gathers #31–40 from line 21X. Orange arrows indicate the positions of the corresponding shot points along the 21X profile. Within these shot gathers, a prominent reflection at a two-way travel time (TWT) of approximately 1.2 s is interpreted as the glacier–lake interface, followed by a ghost reflection 20–30 ms later. A second reflection, observed at a TWT of 1.3 s, is attributed to the lake–bed interface. In some end-shot gathers, such as shot gather #33, linear noise signals interfere with the glacier–lake interface signal, complicating interpretation.

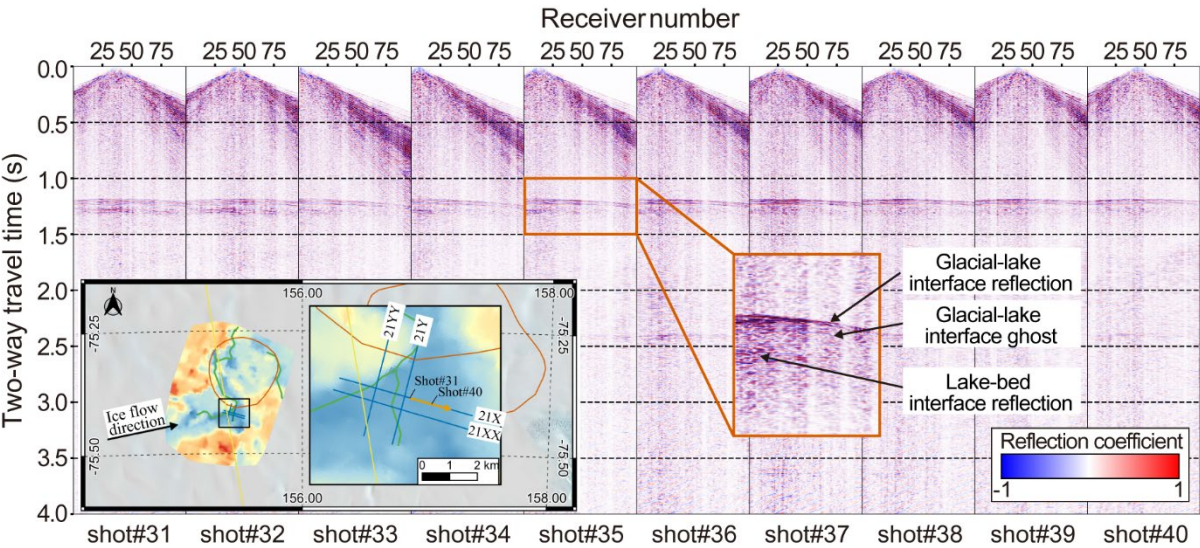


Figure 4: Raw shot gathers (#31–40) from line 21X, with data locations indicated by orange arrows.

3.2 Seismic data processing

Although seismic data acquired from glaciers share processing similarities with those of land-based surveys, glaciological factors, such as surface cracks, crevasses, and strong winds, introduce substantial noise that can degrade data quality (Johansen et al., 2011; Zechmann et al., 2018). Among these factors, linear noise generated by crevasses is particularly detrimental, often obscuring key reflections (Dow et al., 2013). Hence, the glacier seismic data underwent multiple data processing sequences focused on linear noise removal (Fig. 5). A geometry setup was performed using the raw data and geometry information. Multiple data processing and noise removal processes were then carried out to increase the signal-to-noise ratio (SNR).

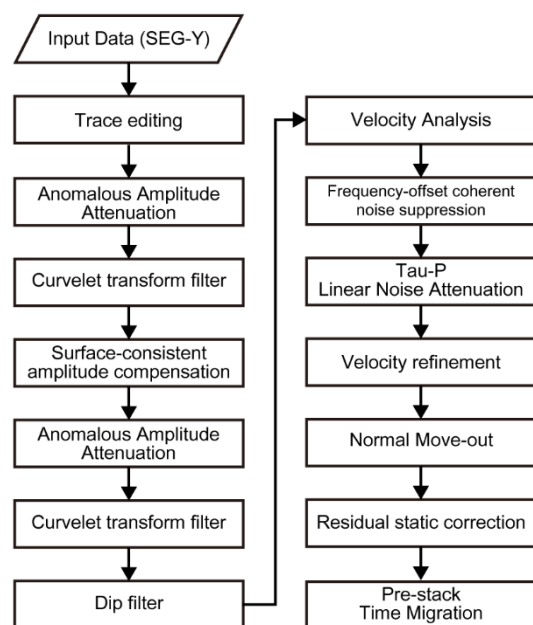


Figure 5: Schematic of the seismic data processing workflow based on the Omega geophysical data processing platform, including noise attenuation, amplitude correction, velocity analysis, and pre-stack time migration.

The initial processing involved anomalous amplitude attenuation (AAA), implemented via a spatial median filter. This step targets outlier amplitudes within a defined frequency band, attenuating anomalous signals through interpolation across neighboring traces. A curvelet transform-based filter was subsequently applied to remove coherent noise. Curvelet decomposition enables the separation of signals based on dip angle and scale, allowing for the selective removal of ground roll and other coherent noise components that differ in dip from true reflections (Oliveira et al., 2012). In this study, linear coherent noise at later arrival times (>2.0 s) was effectively removed using this method.

Surface-consistent amplitude compensation (SCAR) and surface-consistent deconvolution were employed to normalize the amplitude variability across shot gathers. These steps were followed by a second round of AAA and curvelet filtering to suppress artifacts introduced during the compensation and deconvolution stages. Dip filtering was also applied to eliminate spurious hyperbolic arrivals, which were manually identified and removed.

Velocity analysis was conducted at intervals of 40 common mid-points to construct a migration velocity model. Frequency–offset coherent noise suppression (FXCNS) was used to attenuate linear-related noise, followed by Tau-p linear noise attenuation (LNA), effectively reducing the noise associated with crevasse scattering. The final processing steps included velocity model refinement, normal move-out (NMO) correction, and pre-stack time migration (PSTM).

To increase imaging accuracy, a residual static correction was applied before migration using glacier surface elevation data.

The final migrated seismic section was produced using Kirchhoff PSTM. The migrated data has a center frequency of



approximately 180 Hz. Assuming seismic wave velocities between 1395 m/s and 3800 m/s, the corresponding vertical resolutions range from approximately 2.01 m to 5.27 m. This resolution is adequate for imaging SLD2.

4 Seismic data processing results

Figure 6 presents the PSTM results for the four seismic survey lines. On line 21X (Fig. 6b), a strong, laterally continuous reflection with reverse polarity is observed at 0.3–4.8 km along the profile, and the two-way travel time (TWT) is approximately 1.19 s. This reflection is interpreted as the glacier–lake interface (①). Approximately 25–30 ms below this horizon, a normal-polarity reflection (②) appears, likely representing a ghost signal associated with the primary glacier–lake reflection. A deeper normal-polarity reflection is observed within 2.5–3.1 km at TWTs of 1.27–1.29 s (③), which is interpreted as the lake–bed interface. This is followed by a reverse-polarity reflection 25–30 ms later (④), which is presumed to be the corresponding ghost of the lake–bed interface.

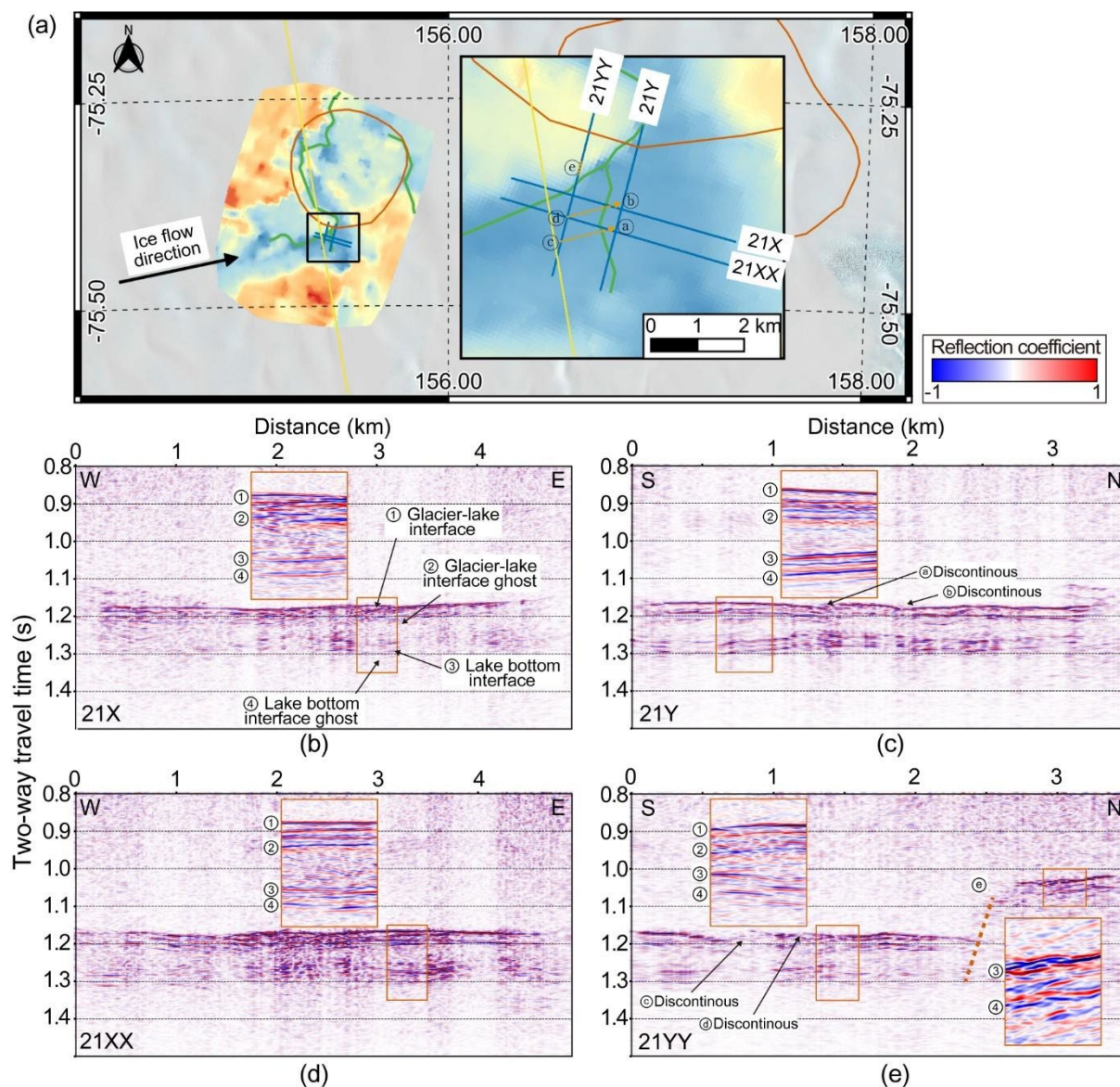


Figure 6: PSTM seismic sections for lines (b) 21X, (c) 21Y, (d) 21XX, and (e) 21YY prior to ghost removal. Ghost reflections appear 25–30 ms beneath the glacier–lake and lake–bed interfaces due to the 25 m source depth.

In line 21Y (Fig. 6c), similar features are observed. A reverse-polarity reflection, interpreted as the glacier–lake interface (①), is observed within 0.1–3.2 km at TWT 1.19 s, with its ghost reflection (②), exhibiting normal polarity, appearing 25–30 ms later. A normal-polarity reflection within 0.1–3.2 km at a TWT of 1.26–1.29 s is interpreted as the lake–bed interface (③), followed by a reverse-polarity ghost signal (④). Additionally, discontinuous reflections interpreted as subglacial scour



features are visible at approximately 1.4 km and 1.9 km along line 21Y at TWT 1.19 s (black arrows in Fig. 6c). These features may be associated with glacial erosion of the underlying substrate.

In line 21XX (Fig. 6d), a reverse-polarity reflection, interpreted as the glacier–lake interface (①), is observed within 0–4.2 km at a TWT of 1.19–1.20 s. This reflection is followed 25–30 ms later by a normal-polarity reflection (②), which is considered the ghost of the primary glacier–lake interface. Further down the section, a normal-polarity reflection (③) within 1.9–4.2 km at a TWT of 1.27–1.29 s is interpreted as the lake–bed interface, followed by its ghost reflection (④) 25–30 ms later.

On line 21YY (Fig. 6e), the glacier–lake interface (①) is marked by a strong, flat, reverse-polarity reflection at 0–2.4 km and a TWT of 1.17–1.19 s, followed by its normal-polarity ghost (②) 25–30 ms below. Lake–bed interface reflections (③) are observed within 0.1–2.4 km at TWTs of 1.27–1.30 s, followed by a reverse-polarity ghost (④) 25–30 ms later. Within 2.4–2.55 km and TWTs of 1.08–1.27 s, no coherent reflection is visible due to the steeply dipping bed topography, as indicated by the dashed orange line in Fig. 6e. Within 2.55–3.5 km and a TWT of 1.02–1.1 s, a stair-step-shaped reflection at the glacier–bed interface (③) is identified, followed by its reverse-polarity ghost (④). Additionally, similar to observations on line 21Y, discontinuous reflections interpreted as scour surfaces appear at 0.7 km and 1.2 km along line 21YY at TWT 1.19 s (black arrows in Fig. 6e).

The discontinuous reflection signals identified on lines 21Y and 21YY are spatially aligned along the ice flow direction when projected laterally (Fig. 6a, dashed orange arrow). This alignment suggests that the observed discontinuities correspond to a subglacial scour surface formed by glacial motion. The scour feature is visible predominantly on lines 21Y and 21YY, which are oriented more perpendicularly to the ice flow direction, thereby enhancing the expression of lateral subglacial variability. In contrast, lines 21X and 21XX are more parallel to the ice flow, resulting in a foreshortened view of the subglacial structures and a relatively flat appearance in the seismic sections (Fig. 7).

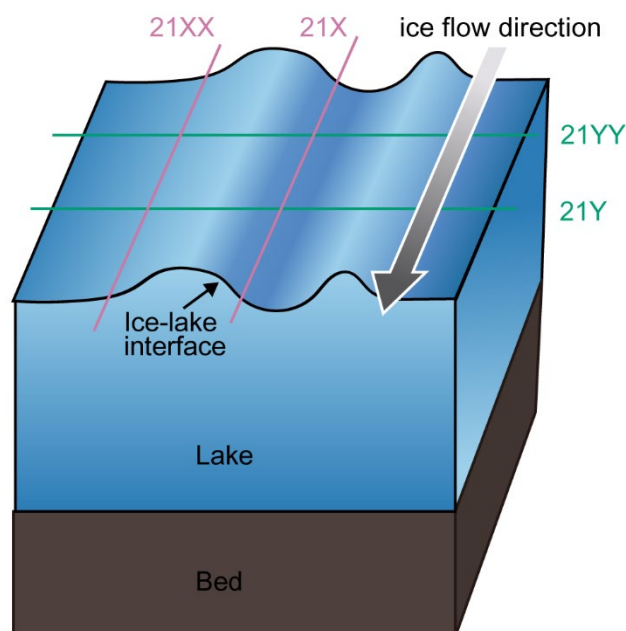


Figure 7: Conceptual diagram illustrating the orientation of seismic survey lines relative to subglacial structures and ice flow direction, explaining the appearance of structural features in each line.

5 Comparison between field data and synthetic seismograms

The depth estimation of subsurface structures from PSTM sections is subject to errors arising primarily from inaccuracies or uncertainties in the seismic velocity model. An inaccurate velocity model may result in erroneous positioning of reflection events, leading to misinterpretation of stratigraphic horizons (Herron, 2000; Yilmaz, 2001). Such limitations are typically mitigated through well-tie analysis, wherein seismic horizons are calibrated against borehole data. However, in the case of SLD2, no borehole data is currently available.

We validate the processed field data by performing a comparative analysis with synthetic seismograms to address this constraint. The forward modeling algorithms based on the staggered grid finite difference method in the time domain were used (Graves et al., 1996). The velocity model for this seismic modeling is constructed by structural information given by the seismic migration sections, integrating published values of P-wave velocities for firn, glacial ice, and subglacial water. P-wave velocities in firn vary from 1525 to 3800 m s⁻¹ because density increases with depth (Kirchner and Bentley, 1979; Picotti et al., 2015; Qin et al., 2024). Glacial ice has an average P-wave velocity of approximately 3800 ± 5 m s⁻¹ at -2 ± 2 °C (Kohnen, 1974), while subglacial water has a velocity of roughly 1396 ± 2 m s⁻¹ at -1.75 ± 0.25 °C, with a salinity less than 1 PSU (practical salinity units) (Thoma et al., 2010; Tulaczyk et al., 2014). Additionally, in line 21YY, the polarity at the ice–bedrock interface is normal, indicating that the P-wave velocity of the bedrock is faster than that of the overlying glacial ice. Therefore,



the bedrock P-wave velocity was set to 4000 m s^{-1} . Using this information, a layered P-wave velocity model comprising firn, glacial ice, subglacial lakes, and bedrock was developed (Fig. 8). Forward modeling was then conducted using the Ricker wavelet, with acquisition parameters matching those used in the field survey (Table 2). The same seismic processing sequence applied to the field data (Section 3.2, Fig. 5) was subsequently applied to the synthetic dataset to produce a PSTM image for comparison.

Table 2: Parameters of the synthetic model.

Synthetic modeling parameters			
Model size	3.5 km (distance) x 3 km (depth)		
Source	Ricker wavelet (zero-phase), 60 Hz 25 m depth, 90-m interval		
Receiver	0 m depth, 15-m interval, 96 channel		
Grid spacing	0.5-m		
Sampling interval	0.1 ms		
Layer parameters	Thickness (m)	Velocity (m/s)	Density (g/cm ³)
Firn	100	1,525–3,800	0.3–0.917
Ice	1,887–2,221	3,800	0.917
Water	0–82±1.3	1,396	1.017
Bed	723–1,113	4,000	2.1

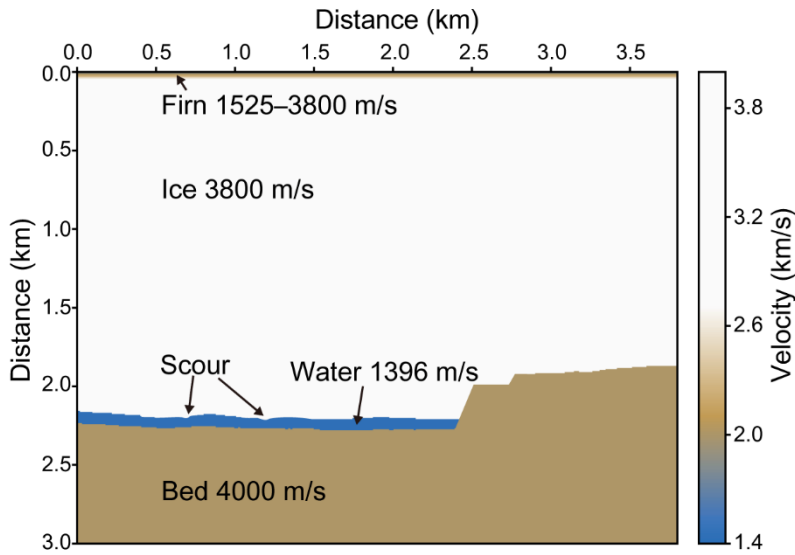


Figure 8: P-wave velocity model used in forward modeling for line 21YY. The upper ~100 m represents firn with velocities ranging from $1525 \text{ to } 3800 \text{ m s}^{-1}$ (Kirchner and Bentley, 1979; Picotti et al., 2015; Qin et al., 2024). The ice below this depth has a velocity of $3800 \pm 5 \text{ m s}^{-1}$ (Kohnen, 1974), and the subglacial water layer has a velocity of $1396 \pm 2 \text{ m s}^{-1}$ (Thoma et al., 2010; Tulaczyk et al., 2014).



Figure 9a compares the shot gather from the synthetic dataset (left) and the corresponding gather from seismic data line 21YY (right) at the same location. A prominent reflection at a TWT of 1.17 s is observed in both datasets, corresponding to the glacier–lake interface (①). This reflection results in a high impedance contrast and reverse polarity due to the P-wave velocity difference between glacial ice and water. These features are consistent with previous observations at glacier–lake interfaces (Atre and Bentley, 1993; Brisbourne et al., 2023; Horgan et al., 2012; King et al., 2004; Peters et al., 2007; Woodward et al., 2010). A secondary reflection with normal polarity appears approximately 28 ms after the primary event (②) and is interpreted as a surface ghost reflection. This time delay corresponds to a generating seismic source depth of approximately 25 m, consistent with previous seismic analyses (Brisbourne et al., 2023; Schlegel et al., 2024). That is, assuming an average P-wave velocity of 1800 m s⁻¹ within the top 25 m, the TWT of the ghost reflection matches the expected delay:

$$TWT_{ghost} = \frac{2 \times 25 \text{ m}}{1800 \text{ m/s}} \approx 28 \text{ ms.}$$

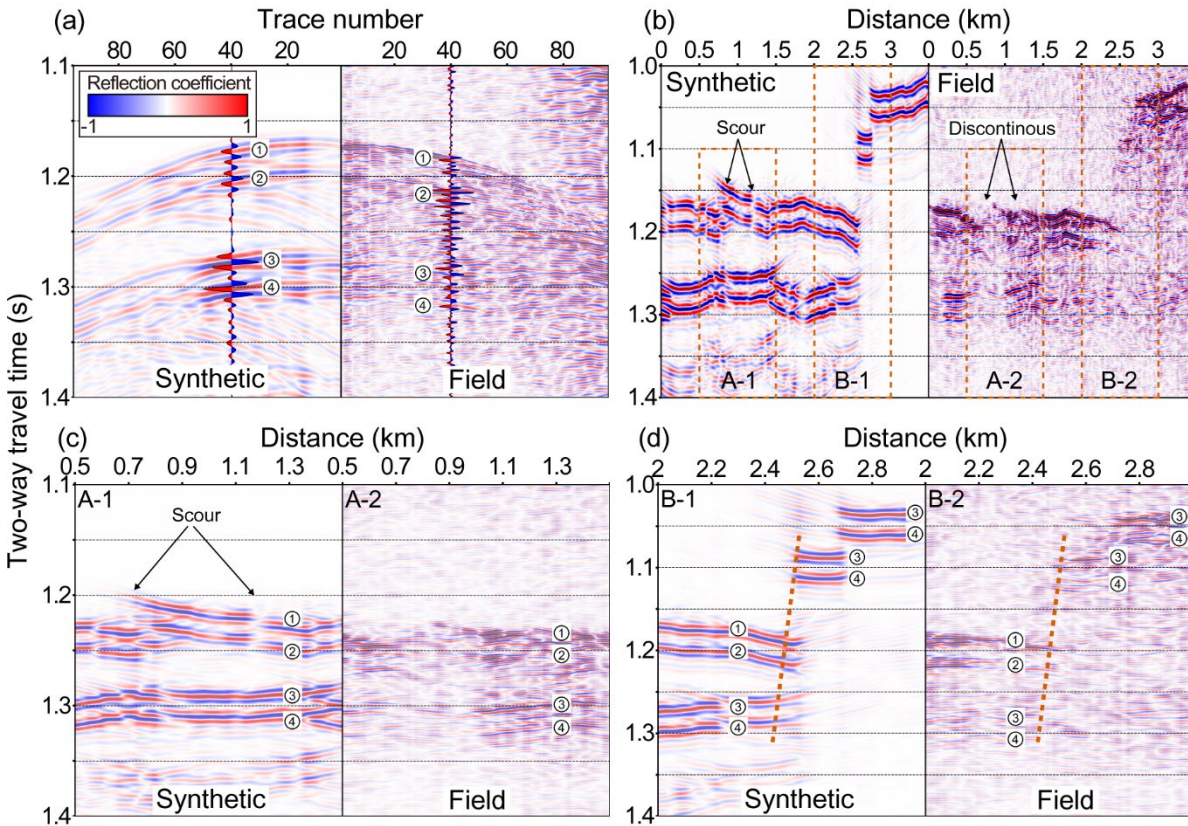


Figure 9: Comparison of synthetic and field seismic data. (a) Shot gather at the same location for synthetic (left) and 21YY field data (right). (b) PSTM comparison between the synthetic model and the 21YY line. (c) Enlarged views of discontinuous reflections (A-1: synthetic, A-2: field). (d) Comparison of dipping bed reflections (B-1: synthetic, B-2: field), showing shadow zones and steep basal topography.



Furthermore, considering that the acoustic impedance of air is approximately zero ($Z_{air} \approx 0$) and that of ice is Z_{ice} , the reflection coefficient (RC) for an upgoing wave at the air–ice interface can be approximated as follows:

$$RC = \frac{Z_{air} - Z_{ice}}{Z_{ice} + Z_{air}} \approx -1. \quad (1)$$

This implies that the polarity of the ghost reflection at the surface is reversed relative to the downgoing primary wave (Krail and Shin, 1990; Robinson and Treitel, 2008).

Figure 9b compares the PSTM sections of the synthetic model (left) and the field data from line 21YY (right). Unlike the field data, the synthetic dataset is free from ambient noise and features a precise source–receiver geometry, resulting in clearer delineation of subsurface reflections and facilitating structural interpretation. The synthetic and field PSTM sections exhibit four principal reflection events (①–④) at identical TWTs. Reflections ① and ④ are characterized by reverse polarity, whereas ② and ③ display normal polarity, which is consistent across both datasets. Discontinuous reflections observed in the synthetic model are interpreted as indicative of a subglacial scour surface.

Figure 9c provides a magnified comparison of regions A-1 (synthetic) and A-2 (field), focusing on discontinuous features. Although the discontinuous reflections and associated low impedance at 0.7 km and 1.2 km (TWT = 1.19 s) in the field data (A-2) are challenging to resolve, the scour surface beneath the glacier is imaged in the synthetic section (A-1).

Figure 9d presents a magnified comparison of regions B-1 (synthetic) and B-2 (field) to examine reflections from a dipping bed. Within 2.4–2.55 km and TWTs of 1.04–1.27 s, reflections are temporally dispersed, resulting in a shadow zone where coherent signals are absent. From 2.0–2.4 km, a reversed-polarity reflection (①) is observed, whereas from 2.55–3.0 km, a normal-polarity reflection (③) is present. The latter is interpreted as the glacier–bed interface. The dashed line traces the steeply dipping bed geometry, delineating the lake margin, with an estimated dip angle of approximately 52° . The resulting shadow zone is likely caused by the lateral scattering of seismic energy along the steep slope. The comparison of synthetic PSTM sections confirms that the velocity model used for seismic imaging appropriately represents the structures of glacial and subglacial lakes.

To further validate the interpretation, ice thickness estimates from the seismic data were compared with those derived from airborne IPR surveys along four seismic lines (Fig. 10) (Frémand et al., 2023; Ju et al., 2024b). Given the lack of spatial coincidence between seismic and IPR profiles, kriging-based two-dimensional interpolation (Isaaks and Srivastava, 1989) was applied to the IPR dataset to estimate the ice thickness at seismic line locations. The uncertainties associated with the IPR and seismic datasets are ± 20.98 m and ± 5.27 m, respectively, resulting in a combined uncertainty of ± 24.05 m. The root mean square error (RMSE) between the two datasets is calculated as ± 29.4 m, exceeding this expected uncertainty range. This discrepancy is attributed primarily to smoothing effects introduced by interpolation in the IPR data, particularly between 1.7 and 2.6 km along line 21YY, within the light blue shaded area in Fig. 10, where seismic data reveal a significantly steeper basal slope. When this localized region is excluded, the RMSE is reduced to ± 24.8 m, approximating the combined uncertainty. Thus, apart from localized artifacts, the seismic and IPR datasets exhibit strong agreement. This consistency supports the



mutual reliability of both methods and validates their integrated application for subglacial lake characterization. Despite localized differences, the overall ice thickness estimates from both datasets are in strong agreement, and this cross-validation reinforces the robustness of the seismic interpretation and affirms the consistency between the two geophysical approaches. As additional supporting evidence for the interpretation, a steeply dipping (approximately 52°) bedrock boundary observed along the 21YY line is consistently identified in both the seismic PSTM profile (Figure 9d) and the IPR-derived ice thickness graph (Figure 10), indicating a similar topographic transition in both datasets. This boundary is interpreted as a structural margin delineating the lateral extent of SLD2 and likely functions as a hydrological barrier. The structural congruence observed in both seismic and radar data underscores the effectiveness of integrating these datasets to delineate the boundaries of subglacial lakes, particularly in regions characterized by complex basal topography.

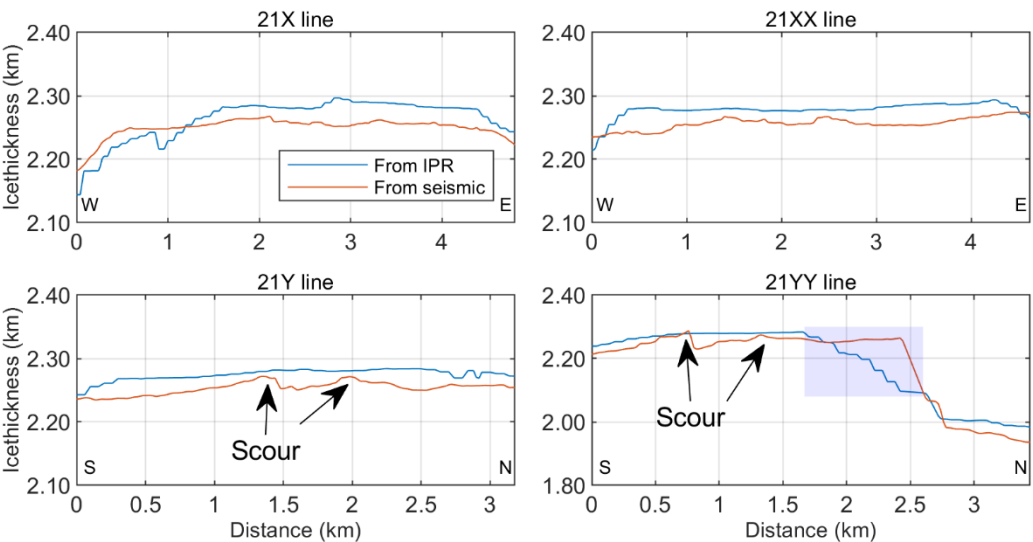


Figure 10: A comparison of ice thickness estimates derived from seismic and kriging-interpolated IPR data (Frémand et al., 2023; Ju et al., 2024b) along the four seismic survey lines reveals high overall consistency between the two datasets, despite localized discrepancies. The light blue shaded region represents areas where interpolation contributes to the divergence between the two measurement approaches.

6 Conclusion

Since 2016, the KOPRI has conducted a series of geophysical investigations to study SLD2 beneath David Glacier, beginning with airborne IPR surveys. In 2021, a seismic survey was carried out to characterize the internal structure and water column of SLD2. The seismic data revealed strong, laterally continuous reflections with reverse polarity at the glacier–lake interface, whereas normal-polarity reflections were observed at the glacier–bed and lake–bed interfaces.



A velocity model was constructed on the basis of seismic interpretation, and synthetic seismic data were generated through wave propagation modeling. A comparison between synthetic and field PSTM sections demonstrated strong agreement in the timing and polarity of major reflection events at the glacier–lake and lake–bed interfaces, confirming the validity of the velocity model. This model estimated the ice thickness and lake water column height to be 2250–2300 m and 53–82 m, respectively. These thickness estimates are in close agreement with independent IPR measurements acquired in 2018, further supporting the reliability of the seismic interpretation.

In lines 21Y and 21YY, discontinuous reflections were observed near the glacier base. The discontinuous signals are interpreted as scour surfaces formed by basal erosion. Structural alignment across multiple survey lines reveals that these features are oriented in the direction of ice flow, supporting the interpretation of glacial erosion processes at the bed.

This study demonstrates the utility of seismic surveys for the structural characterization of subglacial lake environments. The integrated analysis of seismic and synthetic data provides quantitative constraints on the geometry of SLD2 beneath David Glacier. It offers critical insights for future research and logistical planning, including potential subglacial drilling operations.

Data availability

The seismic data and ICESat-2 laser altimetry datasets are available through the Korea Polar Data Center (KPDC) at <https://dx.doi.org/doi:10.22663/KOPRI-KPDC-00001177>. The maps related to Antarctica were created using the Quantarctica dataset version 3.2 (Matsuoka et al., 2018).

Author contribution

HJ: Writing—original draft, investigation, methodology, conceptualization. SGK: Writing—original draft, methodology, conceptualization, supervision. YC: Writing – original draft, data processing, modeling. SP: Data processing methodology. MJL: Writing – original draft. HK: Hot-water drilling. KK: Investigation. YK: Investigation. JIL: Project administration, Funding acquisition.

Competing interests

The authors declare that they have no known competing financial interests or personal relationships that could have appeared to influence the work reported in this paper.

Acknowledgements

We express our sincere gratitude to Sungjun Jeon and the K-route team for their invaluable logistical support. We also extend our appreciation to Do-youn Kwon, Jamin Park, Sanghyeok Seo, and Byeongguk Moon for their dedicated assistance in



seismic surveys.

Financial support

This research was supported by KOPRI grants funded by the Ministry of Oceans and Fisheries (KOPRI project Nos. PE25070).

Additional information.

We name Subglacial Lake D2 Subglacial Lake Cheongsuk (SLC). The name Cheongsuk has a significant meaning, as it is the pen name of Dr. Yeadong Kim, the founder of the Korea Polar Research Institute (KOPRI) and former president of the Scientific Committee on Antarctic Research (SCAR). Dr. Kim personally led the IPR and seismic surveys of Subglacial Lake Cheongsuk and coauthored this paper.

References

- Atre, S. R. and Bentley, C. R.: Laterally varying basal conditions beneath ice Streams B and C, West Antarctica, *J. Glaciol.*, 39, 507–514, <https://doi.org/10.3189/s0022143000016403>, 1993.
- Bell, R. E., Studinger, M., Shuman, C. A., Fahnestock, M. A., and Joughin, I.: Large subglacial lakes in East Antarctica at the onset of fast-flowing ice streams, *Nature*, 445, 904–907, <https://doi.org/10.1038/nature05554>, 2007.
- Bell, R. E., Ferraccioli, F., Creyts, T. T., Braaten, D., Corr, H., Das, I., Damaske, D., Frearson, N., Jordan, T., Rose, K., Studinger, M., and Wolovick, M.: Widespread persistent thickening of the east antarctic ice sheet by freezing from the base, *Science*, 331, 1592–1595, <https://doi.org/10.1126/science.1200109>, 2011.
- Bentley, M. J., Hodgson, D. A., Smith, J. A., Cofaigh, C. Ó., Domack, E. W., Larter, R. D., Roberts, S. J., Brachfeld, S., Leventer, A., Hjort, C., Hillenbrand, C. D., and Evans, J.: Mechanisms of Holocene palaeoenvironmental change in the Antarctic Peninsula region, *Holocene*, 19, 51–69, <https://doi.org/10.1177/0959683608096603>, 2009.
- Brisbourne, A. M., Smith, A. M., Rivera, A., Zamora, R., Napoleoni, F., Uribe, J. A., and Ortega, M.: Bathymetry and bed conditions of Lago Subglacial CECs, West Antarctica, *J. Glaciol.*, 69, 1–10, <https://doi.org/10.1017/jog.2023.38>, 2023.
- Christianson, K., Jacobel, R. W., Horgan, H. J., Anandakrishnan, S., and Alley, R. B.: Subglacial Lake Whillans — Ice-penetrating radar and GPS observations of a shallow active reservoir beneath a West Antarctic ice stream, *Earth Planet. Sc. Lett.*, 331–332, 237–245, <https://doi.org/10.1016/j.epsl.2012.03.013>, 2012.
- Christner, B. C., Priscu, J. C., Achberger, A. M., Barbante, C., Carter, S. P., Christianson, K., Michaud, A. B., Mikucki, J. A., Mitchell, A. C., Skidmore, M. L., Vick-Majors, T. J., Adkins, W. P., Anandakrishnan, S., Barcheck, G., Beem, L., Behar, A., Beitch, M., Bolsey, R., Branecky, C., Edwards, R., Fisher, A., Fricker, H. A., Foley, N., Guthrie, B., Hodson, T., Horgan, H., Jacobel, R., Kelley, S., Mankoff, K. D., McBryan, E., Powell, R., Purcell, A., Sampson, D., Scherer, R., Sherve, J., Siegfried, M., and Tulaczyk, S.: A microbial ecosystem beneath the West Antarctic ice sheet, *Nature*, 512, 310–313, <https://doi.org/10.1038/nature13667>, 2014.



- Dow, C. F., Hubbard, A., Booth, A. D., Doyle, S. H., Gusmeroli, A., and Kulesa, B.: Seismic evidence of mechanically weak sediments underlying Russell Glacier, West Greenland, *Ann. Glaciol.*, 54, 135–141, <https://doi.org/10.3189/2013aog64a032>, 2013.
- Engelhardt, H., Humphrey, N., Kamb, B., and Fahnestock, M.: Physical conditions at the base of a fast moving Antarctic ice stream, *Science*, 248, 57–59, <https://doi.org/10.1126/science.248.4951.57>, 1990.
- Filina, I. Y., Blankenship, D. D., Thoma, M., Lukin, V. V., Masolov, V. N., and Sen, M. K.: New 3D bathymetry and sediment distribution in Lake Vostok: implication for pre-glacial origin and numerical modeling of the internal processes within the lake, *Earth Planet. Sc. Lett.*, 276, 106–114, <https://doi.org/10.1016/j.epsl.2008.09.012>, 2008.
- Frémand, A. C., Fretwell, P., Bodart, J. A., Pritchard, H. D., Aitken, A., Bamber, J. L., Bell, R., Bianchi, C., Bingham, R. G., Blankenship, D. D., Casassa, G., Catania, G., Christianson, K., Conway, H., Corr, H. F. J., Cui, X., Damaske, D., Damm, V., Drews, R., Eagles, G., Eisen, O., Eisermann, H., Ferraccioli, F., Field, E., Forsberg, R., Franke, S., Fujita, S., Gim, Y., Goel, V., Gogineni, S. P., Greenbaum, J., Hills, B., Hindmarsh, R. C. A., Hoffman, A. O., Holmlund, P., Holschuh, N., Holt, J. W., Horlings, A. N., Humbert, A., Jacobel, R. W., Jansen, D., Jenkins, A., Jokat, W., Jordan, T., King, E., Kohler, J., Krabill, W., Kusk Gillespie, M., Langley, K., Lee, J., Leitchenkov, G., Leuschen, C., Luyendyk, B., MacGregor, J., MacKie, E., Matsuoka, K., Morlighem, M., Mouginot, J., Nitsche, F. O., Nogi, Y., Nost, O. A., Paden, J., Pattyn, F., Popov, S. V., Rignot, E., Rippin, D. M., Rivera, A., Roberts, J., Ross, N., Ruppel, A., Schroeder, D. M., Siegert, M. J., Smith, A. M., Steinhage, D., Studinger, M., Sun, B., Tabacco, I., Tinto, K., Urbini, S., Vaughan, D., Welch, B. C., Wilson, D. S., Young, D. A., and Zirizzotti, A.: Antarctic bedmap data: findable, accessible, interoperable, and reusable (FAIR) sharing of 60 years of ice bed, surface, and thickness data, *Earth Syst. Sci. Data*, 15, 2695–2710, <https://doi.org/10.5194/essd-15-2695-2023>, 2023.
- Frezzotti, M., Tabacco, I. E., and Zirizzotti, A.: Ice discharge of eastern Dome C drainage area, Antarctica, determined from airborne radar survey and satellite image analysis, *J. Glaciol.*, 46, 253–264, <https://doi.org/10.3189/172756500781832855>, 2000.
- Graves, R. W.: Simulating seismic wave propagation in 3D elastic media using staggered-grid finite differences, *Bulletin of the seismological society of America*, 86, 1091–1106, <https://doi.org/10.1785/BSSA0860041091>, 1996.
- Herron, D. A.: Pitfalls in seismic interpretation: depth migration artifacts, *The Leading Edge*, 19, 1016–1017, <https://doi.org/10.1190/1.1438756>, 2000.
- Horgan, H. J., Anandakrishnan, S., Jacobel, R. W., Christianson, K., Alley, R. B., Heeszel, D. S., Picotti, S., and Walter, J. I.: Subglacial Lake Whillans — Seismic observations of a shallow active reservoir beneath a West Antarctic ice stream, *Earth Planet. Sc. Lett.*, 331–332, 201–209, <https://doi.org/10.1016/j.epsl.2012.02.023>, 2012.
- Isaaks, E. H. and Srivastava, R. M.: *An Introduction to Applied Geostatistics*, Oxford University Press, Oxford, 1989.
- Johansen, T. A., Ruud, B. E., Bakke, N. E., Riste, P., Johannessen, E. P., and Henningsen, T.: Seismic profiling on Arctic glaciers, *First Break*, 29, 65–71, <https://doi.org/10.3997/1365-2397.20112st1>, 2011.
- Ju, H., Choi, Y., and Kang, S.-G.: Seismic Survey for the Subglacial Lake in Antarctica. *Geophysics and Geophysical Exploration*, 27, 244–257. <https://doi.org/10.7582/gge.2024.27.4.244>, 2024a.
- Ju, H., Lee, J., Lee, J., and Blankenship, D. D.: Air borne Ice radar survey data and Space borne satellite data of Korean route from David glacier, Antarctica in 2018 [Dataset]. <https://doi.org/10.22663/kopri-kpdc-00001177>, 2024b.



- King, E. C., Woodward, J., and Smith, A. M.: Seismic evidence for a water-filled canal in deforming till beneath Rutford Ice Stream, West Antarctica, *Geophys. Res. Lett.*, 31, L20401, <https://doi.org/10.1029/2004gl020379>, 2004.
- Kirchner, J. F. and Bentley, C. R.: Seismic short-refraction studies on the Ross Ice Shelf, Antarctica, *J. Glaciol.*, 24, 313–319, <https://doi.org/10.3189/s0022143000014830>, 1979.
- Kohnen, H.: The temperature dependence of seismic waves in ice, *J. Glaciol.*, 13, 144–147, <https://doi.org/10.3189/s0022143000023467>, 1974.
- Krail, P. M. and Shin, Y.: Deconvolution of a directional marine source, *Geophysics*, 55, 1542–1548, <https://doi.org/10.1190/1.1442805>, 1990.
- Lindzey, L. E., Beem, L. H., Young, D. A., Quartini, E., Blankenship, D. D., Lee, C.-K., Lee, W. S., Lee, J. I., and Lee, J.: Aerogeophysical characterization of an active subglacial lake system in the David Glacier catchment, Antarctica, *Cryosphere*, 14, 2217–2233, <https://doi.org/10.5194/tc-14-2217-2020>, 2020.
- Livingstone, S. J., Li, Y., Rutishauser, A., Sanderson, R. J., Winter, K., Mikucki, J. A., Björnsson, H., Bowling, J. S., Chu, W., Dow, C. F., Fricker, H. A., McMillan, M., Ng, F. S. L., Ross, N., Siegert, M. J., Siegfried, M., and Sole, A. J.: Subglacial lakes and their changing role in a warming climate, *Nature Reviews Earth & Environment*, 3, 106–124, <https://doi.org/10.1038/s43017-021-00246-9>, 2022.
- Matsuoka, K., Skoglund, A., Roth, G., de Pomereu, J., Griffiths, H., Headland, R., Herried, B., Katsumata, K., Le Brocq, A., Licht, K., Morgan, F., Neff, P., Ritz, C., Scheinert, M., Tamura, T., Van de Putte, A., van den Broeke, M., von Deschanden, A., Deschamps-Berger, C., ... Melvær, Y.: Quantarctica [Dataset]. Norwegian Polar Institute. <https://doi.org/10.21334/NPOLAR.2018.8516E961>, 2018.
- Oliveira, M. S., Henriques, M. V. C., Leite, F. E. A., Corso, G., and Lucena, L. S.: Seismic denoising using curvelet analysis, *Physica A*, 391, 2106–2110, <https://doi.org/10.1016/j.physa.2011.04.009>, 2012.
- Peters, L. E., Anandakrishnan, S., Alley, R. B., and Smith, A. M.: Extensive storage of basal meltwater in the onset region of a major West Antarctic ice stream, *Geology*, 35, 251–254, <https://doi.org/10.1130/g23222a.1>, 2007.
- Picotti, S., Vuan, A., Carcione, J. M., Horgan, H. J., and Anandakrishnan, S.: Anisotropy and crystalline fabric of Whillans Ice Stream (West Antarctica) inferred from multicomponent seismic data, *J. Geophys. Res. Sol. Ea.*, 120, 4237–4262, <https://doi.org/10.1002/2014jb011591>, 2015.
- Priscu, J. C. and Christner, B. C.: Earth's icy biosphere, in: *Microbial Diversity and Bioprospecting*, edited by: Bull, A. T., ASM Press, Washington, D.C, 130–145, <https://doi.org/10.1128/9781555817770.ch13>, 2003.
- Qin, L., Qiu, H., Nakata, N., Booth, A., Zhang, Z., Karplus, M., McKeague, J., Clark, R., and Kaip, G.: High-resolution characterization of the firn layer near the West Antarctic ice sheet divide camp with active and passive seismic data, *Geophys. Res. Lett.*, 51, e2024GL108933, <https://doi.org/10.1029/2024gl108933>, 2024.
- Rignot, E., Mouginot, J., Scheuchl, B., van den Broeke, M., van Wessem, M. J., and Morlighem, M.: Four decades of Antarctic Ice Sheet mass balance from 1979–2017, *P. Natl. Acad. Sci. USA*, 116, 1095–1103, <https://doi.org/10.1073/pnas.1812883116>, 2019.
- Robinson, E. A. and Treitel, S.: *Digital Imaging and Deconvolution*, Society of Exploration Geophysicists, Tulsa, Okla, 2008.
- Rose, K. E.: Characteristics of ice flow in Marie Byrd Land, Antarctica, *J. Glaciol.*, 24, 63–75, <https://doi.org/10.3189/s0022143000014659>, 1979.
- Schlegel, R., Brisbourne, A. M., Smith, A. M., Booth, A. D., Murray, T., King, E. C., and Clark, R. A.: Subglacial bedform and moat initiation beneath Rutford Ice Stream, West Antarctica, *Geomorphology*, 458, 109207, <https://doi.org/10.1016/j.geomorph.2024.109207>, 2024.



- Siegfried, M. R. and Fricker, H. A.: Thirteen years of subglacial lake activity in Antarctica from multi-mission satellite altimetry, *Ann. Glaciol.*, 59, 42–55, <https://doi.org/10.1017/aog.2017.36>, 2018.
- Smith, A. M., Woodward, J., Ross, N., Bentley, M. J., Hodgson, D. A., Siegert, M. J., and King, E. C.: Evidence for the long-term sedimentary environment in an Antarctic subglacial lake, *Earth Planet. Sc. Lett.*, 504, 139–151, <https://doi.org/10.1016/j.epsl.2018.10.011>, 2018.
- Smith, B. E., Fricker, H. A., Joughin, I. R., and Tulaczyk, S.: An inventory of active subglacial lakes in Antarctica detected by ICESat (2003–2008), *J. Glaciol.*, 55, 573–595, <https://doi.org/10.3189/002214309789470879>, 2009.
- Stearns, L. A., Smith, B. E., and Hamilton, G. S.: Increased flow speed on a large East Antarctic outlet glacier caused by subglacial floods, *Nat. Geosci.*, 1, 827–831, <https://doi.org/10.1038/ngeo356>, 2008.
- Thoma, M., Grosfeld, K., Smith, A. M., and Mayer, C.: A comment on the Equation of State and the freezing point equation with respect to subglacial lake modelling, *Earth Planet. Sc. Lett.*, 294, 80–84, <https://doi.org/10.1016/j.epsl.2010.03.005>, 2010.
- Tulaczyk, S., Mikucki, J. A., Siegfried, M. R., Priscu, J. C., Barcheck, C. G., Beem, L. H., Behar, A., Burnett, J., Christner, B. C., Fisher, A. T., Fricker, H. A., Mankoff, K. D., Powell, R. D., Rack, F., Sampson, D., Scherer, R. P., and Schwartz, S. Y.: WISSARD at Subglacial Lake Whillans, West Antarctica: scientific operations and initial observations, *Ann. Glaciol.*, 55, 51–58, <https://doi.org/10.3189/2014aog65a009>, 2014.
- Voigt, D. E., Peters, L. E., and Anandakrishnan, S.: ‘Georods’: the development of a four-element geophone for improved seismic imaging of glaciers and ice sheets, *Ann. Glaciol.*, 54, 142–148, <https://doi.org/10.3189/2013aog64a432>, 2013.
- Wingham, D. J., Siegert, M. J., Shepherd, A., and Muir, A. S.: Rapid discharge connects Antarctic subglacial lakes, *Nature*, 440, 1033–1036, <https://doi.org/10.1038/nature04660>, 2006.
- Winsborrow, M. C. M., Clark, C. D., and Stokes, C. R.: What controls the location of ice streams?, *Earth-Sci. Rev.*, 103, 45–59, <https://doi.org/10.1016/j.earscirev.2010.07.003>, 2010.
- Woodward, J., Smith, A. M., Ross, N., Thoma, M., Corr, H. F. J., King, E. C., King, M. A., Grosfeld, K., Tranter, M., and Siegert, M. J.: Location for direct access to subglacial Lake Ellsworth: an assessment of geophysical data and modeling, *Geophys. Res. Lett.*, 37, L11501, <https://doi.org/10.1029/2010gl042884>, 2010.
- Wright, A. and Siegert, M.: A fourth inventory of Antarctic subglacial lakes, *Antarct. Sci.*, 24, 659–664, <https://doi.org/10.1017/s095410201200048x>, 2012.
- Yan, S., Blankenship, D. D., Greenbaum, J. S., Young, D. A., Li, L., Rutishauser, A., Guo, J., Roberts, J. L., van Ommen, T. D., Siegert, M. J., and Sun, B.: A newly discovered subglacial lake in East Antarctica likely hosts a valuable sedimentary record of ice and climate change, *Geology*, 50, 949–953, <https://doi.org/10.1130/g50009.1>, 2022.
- Yilmaz, Ö.: *Seismic Data Analysis: Processing, Inversion, and Interpretation of Seismic Data*, Society of Exploration Geophysicists, Tulsa, Okla, 2001.
- Zechmann, J. M., Booth, A. D., Truffer, M., Gusmeroli, A., Amundson, J. M., and Larsen, C. F.: Active seismic studies in valley glacier settings: strategies and limitations, *J. Glaciol.*, 64, 796–810, <https://doi.org/10.1017/jog.2018.69>, 2018.